Cell, Vol. 103, 981–991, December 8, 2000, Copyright ©2000 by Cell Press

Gradient Formation of the TGF-β Homolog Dpp

Eugeni V. Entchev,*† Anja Schwabedissen,*† and Marcos González-Gaitán*†‡

*Max-Planck-Institut für molekulare Zellbiologie und Genetik
Pfotenhauerstrasse, 108
D-01307 Dresden
Germany

†Max-Planck-Institut für biophysikalische Chemie
Am Fassberg, 11
D-37077 Göttingen
Germany

Summary

Secreted morphogens such as the *Drosophila* TGF-β homolog Decapentaplegic (Dpp) are thought to spread through target tissues and form long-range concentration gradients providing positional information. Using a GFP-Dpp fusion, we monitored a TGF-β family member trafficking in situ throughout the target tissue and forming a long-range concentration gradient. Evidence is presented that long-range Dpp movement involves Dpp receptor and Dynamin functions. We also show that the rates of endocytic trafficking and degradation determine Dpp signaling range. We propose a model where the gradient is formed via intracellular trafficking initiated by receptor-mediated endocytosis of the ligand in receiving cells with the gradient slope controlled by endocytic sorting of Dpp toward recycling versus degradation.

Introduction

During pattern formation and organogenesis, cells acquire information about their location within a field of equivalent cells and differentiate according to their position. In Wolpert's positional information model (Wolpert, 1969), a "form generating substance" (Turing, 1952), a morphogen, emanates from its source, diffuses across the target field and forms a long-range concentration gradient. Receiving cells interpret the gradient by activating target gene expression at discrete concentration thresholds thereby acquiring positional information. From insects to vertebrates, signaling molecules of the TGF-β family have been shown to act as bona fide morphogens with long-range organizing properties (Green and Smith, 1990; Gurdon et al., 1994; Ingham and Fietz, 1995).

In *Drosophila*, the TGF-β homolog Dpp (Padgett et al., 1987) functions as a morphogen required to specify cell fates along the anterior/posterior (A/P) axis of the wing (Ingham and Fietz, 1995). Dpp is expressed in a stripe of anterior wing cells at the A/P compartment boundary (Basler and Struhl, 1994). It forms a long-range activity gradient necessary for activation of the target genes *spalt* (*sal*) and *optomotorblind* (*omb*) at different distances from the source (Lecuit et al., 1996; Nellen et al., 1996). Based on its long-range *activity* gradient, it has been suggested that Dpp is distributed in a *concentration* gradient. However, antibodies to monitor the distribution of Dpp or any other TGF-β-like factor are not available.

Gurdon and colleagues were able to show that the TGF-β homolog Activin forms a concentration gradient by passive diffusion (McDowell et al., 1997). In the case of Dpp, however, recent reports argue against such a simple mechanism and suggest that factors such as the Dpp type I receptor Thickveins (Lecuit and Cohen, 1998), endocytosis (González-Gaitán and Jäckle, 1999), and cytonemes (Ramírez-Weber and Kornberg, 1999) shape the Dpp activity gradient. These studies point to the necessity of directly monitoring the distribution and trafficking of Dpp to approach the cellular and molecular basis of gradient formation. Here we show Dpp tissue distribution, subcellular localization, and trafficking in the receiving cells.

Results

Tagged Dpp Is a Functional Ligand

GFP was fused to the Dpp mature peptide (Panganiban et al., 1990) which is processed in secreting cells (Figure 1a). It resulted in a stable chimeric GFP-Dpp protein (see Experimental Procedures) allowing us to monitor the traffic of secreted Dpp in the target tissue by GFP fluorescence after fixation or in vivo (Figure 1b). To determine whether GFP-Dpp signals like endogenous Dpp, we performed rescue experiments (Figures 1c–1g) in the dpp^{d12}/dpp^{d14} mutant (Masucci et al., 1990). This mutant lacks *dpp* and *sal* target gene expression in the wing (Lecuit et al., 1996) (Figure 1d), dies during early puparation, and fails to differentiate epidermal adult structures (Bryant, 1988). GFP-Dpp driven by a Dpp wing promotor in dpp^{d12}/dpp^{d14} elicits Sal expression over the same range as endogenous Dpp (about 15 cell diameters in the posterior compartment; Figures 1c and 1e) and restores normal epidermal structures (Figures 1f and 1g). These flies fail to hatch from their pupal case, as had been observed after rescue with a wild-type Dpp transgene in place of GFP-Dpp (Masucci et al., 1990). This indicates that GFP-Dpp can functionally replace endogenous Dpp, implying that GFP-Dpp can signal and is properly processed and distributed.

GFP-Dpp Forms a Long-Range Gradient

Secreted GFP-Dpp spreads beyond the Dpp secreting cells into the target tissue (Figures 2a–2d). Both in vivo and after fixation, GFP-Dpp is seen up to 80 μm away from the source of GFP-Dpp synthesis in apical intracellular punctate structures within the top 5 μm of the wing epithelium (Figures 2e–2g, and j). Over a range of around 15 μm, GFP-Dpp is also found basolaterally, around 10 μm below the top, appearing both as intracellular punctate structures and in the extracellular space (Fig-

‡To whom correspondence should be addressed (e-mail: mconzal@gwdg.de).

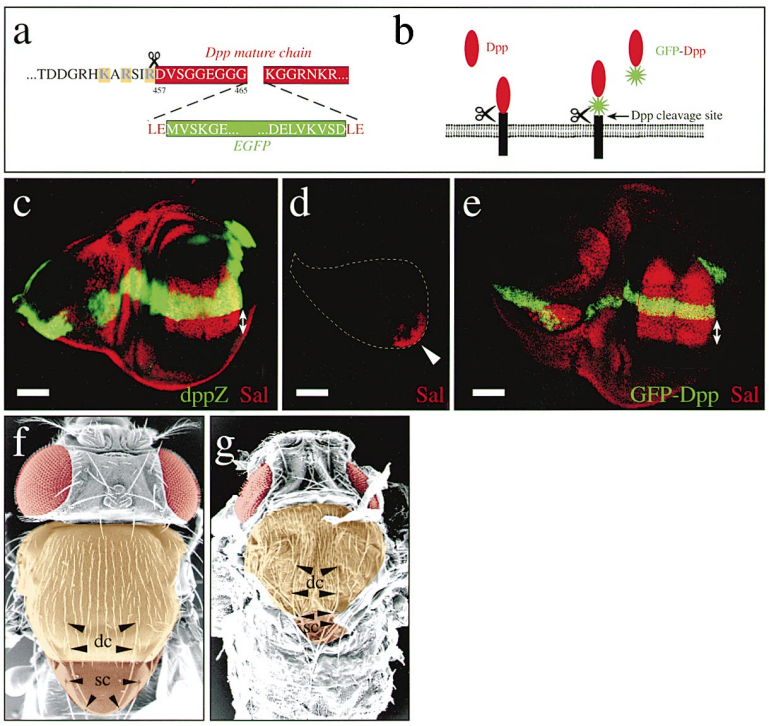

Figure 1. GFP-Dpp Rescues Dpp Mutants

(a) Location of EGFP in the fusion. Green: EGFP; red: Dpp; yellow: furin cleavage site (Cui et al., 1998). (b) Internal insertion of GFP downstream of the furin site (scissors) to tag secreted Dpp (right). (c) Double immunolabeling showing dpp-*lacZ* (green) and *sal* (red) range of activation (arrow). Note Dpp-independent *sal* expression outside the wing pouch. Broad dpp-lacZ stripe is due to long β-Gal perdurance. Anterior: up; dorsal: left. (d) Sal immunostaining (red) in dpp^{d12}/dpp^{d14}. Note that wing expression of Sal is missing; Dpp-independent expression remains (arrowhead). Dashed line: disc profile. (e) Sal immunostaining (red) and GFP-Dpp (green) in a dpp^{d12}/dpp^{d14}; *dpp-gal4/UAS-GFP-Dpp* disc. Note wild-type-like *sal* activation range in the posterior compartment (arrow). Expanded anterior expression of Sal is probably due to perdurance of Gal4 expressed in previous cell generations and/or overexpression of GFP-Dpp. (f) SEM image of a wild-type fly. Eyes (red) and wing disc derivatives (brown) are colored; scutum (light) and scutellum (dark). Note the pattern of micro- and macrobristles. Dorsocentral, dc; scutelar, sc. (g) SEM image of a dpp^{d12}/dpp^{d14}; *dpp-gal4/UAS-GFP-Dpp* fly. Note the rescue as shown by the wild-type-like derivatives of the eye-antennal (eyes, red), wing (scutum and scutellum, brown) and leg imaginal discs (not shown) and abdomen. Note the normal pattern of bristles. Wing veins and the triple row of bristles can be seen in the unfolded wings (not shown). Scale bars: 50 μm (c–e).

ure 2h). Extracellular GFP-Dpp can also be detected with a specific protocol (Strigini and Cohen, 2000) as weak staining delineating the cell profiles adjacent to the Dpp source (Figure 2i). Extracellular GFP-Dpp may also be present at low concentrations far away from the source where it can only be seen when internalized and sufficiently concentrated for detection in an intracellular compartment.

Intracellular apical GFP-Dpp appears as a long-range gradient (Figure 2e–2g, and 2j) where fluorescence decays with the distance to the source (Figure 2k). GFP-Dpp is found beyond the *sal* expression domain (Figure 2l–2n) throughout the region where Dpp is known to elicit signaling (up to 25 cell diameters from its source; Figures 2e and 2f; Lecuit et al., 1996; Nellen et al., 1996). Therefore, Dpp forms a long-range gradient as previously inferred from its concentration-dependent long-range activity (Lecuit et al., 1996; Nellen et al., 1996).

We next asked whether a long-range Dpp gradient can be formed by diffusion through the extracellular space. For this, we monitored the distribution of a secreted GFP fusion protein (sGFP). sGFP is composed of GFP and Dpp sequences including Dpp cleavage and secretory transport domains, but lacks the mature Dpp peptide, which was replaced by a stuffer of the same size (see Experimental Procedures). Like GFP-Dpp, sGFP is secreted and spreads into the developing target tissue. However, it fails to form a gradient and fills the apical extracellular space (Figures 2o and 2p), indicating that diffusion alone cannot explain Dpp gradient formation.

Dynamics of GFP-Dpp Gradient Formation

Based on the slow expansion of the *spalt* expression domain during the last three days of larval development, formation of the Dpp gradient has been suggested to be a long-term process (Lecuit and Cohen, 1998). We monitored the GFP-Dpp pattern during different larval stages. During second instar, GFP-Dpp is found only 5 cell diameters away from its source (Figures 3a and 3b). During early third instar, the gradient is expanded to 10 cells (Figures 3a and 3c) and in late third instar larva, to 25 cells (Figures 3a and 3d). Thus, as the wing grows, the range of the Dpp gradient expands slowly. The rate is less than 2 cells per 5 hr (around 25 cells in 3 days), consistent with the rate of expansion of Dpp signaling range during development (Lecuit and Cohen, 1998).

The rate of Dpp gradient expansion (around 6 μm in 5 hr) is much slower than the speed of Activin diffusion (300 μm in few hours; Gurdon et al., 1994). Capitalizing on the thermosensitivity of Gal4 activity in *Drosophila* (Brand et al., 1996), we studied the speed of Dpp directly. At 16°C, Gal4-driven GFP-Dpp is expressed at low levels and few or no GFP-Dpp punctate structures were found in receiving cells (Figure 3e). This situation allowed us to monitor the speed of Dpp by pulsing GFP-Dpp expression through a temperature shift from 16°C to 25°C and determining in a chase experiment how far Dpp travels in a given time period (Figures 3f–3j). When third instar larvae were shifted from 16°C to 25°C for one hour, few punctate GFP-Dpp appeared in receiving cells adjacent to the source (Figures 3f and 3i). After 2 hr at 25°C, GFP-Dpp could be found up to 12 cells away from

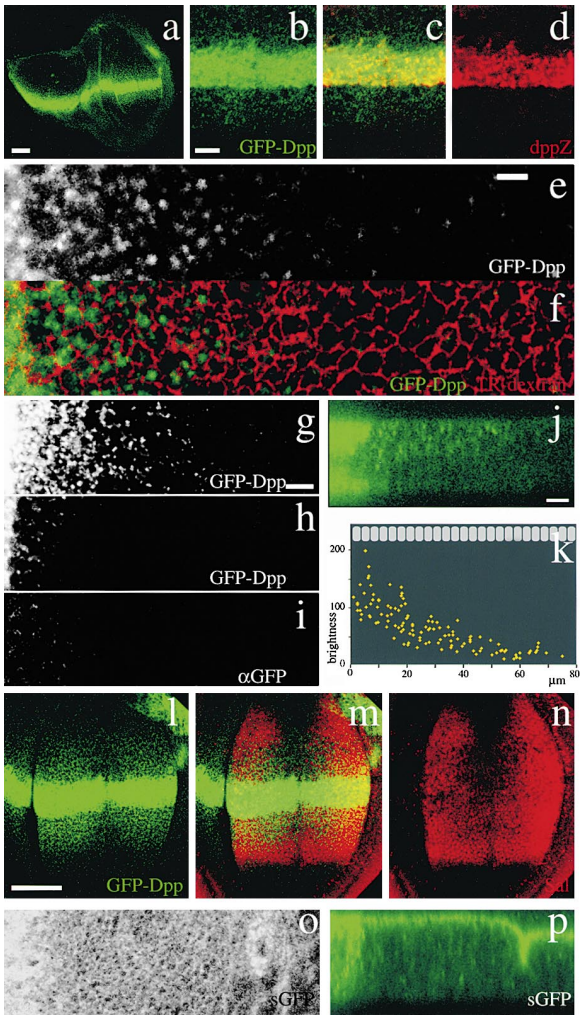

Figure 2. GFP-Dpp Gradient

(a) GFP-Dpp distribution from the Dpp domain (*dpp-gal4/UAS-GFP-Dpp*). (b–d) Double labeling showing GFP-Dpp (b, green) and the Dpp expressing cells, monitored by immunostaining of cytosolic lacZ (d, red). (c) Overlay. Genotype *UAS-lacZ/+; dpp-gal4/UAS-GFP-Dpp*. Note GFP-Dpp punctate structures in receiving cells (b and c) beyond the Dpp expression domain (c and d). The different GFP-Dpp subcellular distribution and levels of accumulation in the secreting and receiving cells are diagnostic markers to identify the receiving cells. (e and f) Double labeling showing an apical confocal section (5 μm from top; in vivo) of a wing disc expressing GFP-Dpp in the Dpp domain (e, green in f) and the cell profiles (f, red) marked by extracellular Texas-red dextran (see Experimental Procedures). Posterior: right; ventral: up. (g–i) Double labeling showing GFP-Dpp (g and h) and immunostaining of extracellular GFP-Dpp by incubating with anti-GFP antibody prior to fixation (i). Apical (3 μm from top, g) and basolateral (10 μm from top; h and i) confocal sections of the same disc. Dpp secreting cells: left. (j) Z section perpendicular to the Dpp domain. Apical: up. Dpp secreting cells: left. (k) Brightness of punctate structures related to their distance to the source in a representative disc. X axis, distance to the source. Top: approximate epithelial cell size; Y axis, brightness of the punctate structure (estimated with NIH image software; 0 to 255 units). (l–n) Double labeling showing GFP-Dpp distribution (l) and Sal immunostaining (n). (m) Overlay. (o and p) Apical (5 μm from top; o) and a Z (p) confocal section of a wing disc expressing sGFP in the Dpp domain (left). sGFP accumulates extracellularly at the apical pole of the epithelium and is not distributed as a gradient. Some dots in (p) represent internalized GFP. Scale bars: 50 μm (a, l–n), 20 μm (b–d), 5 μm (e and f), and 10 μm (g–j, o, and p).

the source (Figures 3g and 3i) and after 4 hr, up to 20 cells (Figures 3h and 3i). This indicates that Dpp moves rapidly, at a speed of more than 4 cells per hour. The range of GFP-Dpp after 4 hr is similar to the one in animals constantly kept at 25°C (Figures 3d, 3h, and 3j). Furthermore, the gradient reaches its full extent and the steady-state between 6 and 8 hr (not shown).

Dpp is not efficiently directed away from the source as shown by GFP-Dpp ectopic expression in small cell clones (Figures 3k, 3l, and 3n). We found GFP-Dpp in all directions around the clone, indicating that GFP-Dpp propagates to all sides. Consistently, we observed *sal* expression surrounding the GFP-Dpp-expressing cell clones (Figures 3m and 3n).

These results show that Dpp moves rapidly and undirected. Therefore, the slow gradient expansion during development does not reflect the actual speed of Dpp. If Dpp moves so rapidly, how can the gradient be stable and expand only slowly during development? Which mechanisms underlie Dpp movement through the tissue? What restricts its propagation?

GFP-Dpp Internalization by Dynamin-Mediated Endocytosis

Notch, Wingless, and Epidermal Growth Factor signaling require Dynamin-mediated endocytosis (Bejsovec and Wieschaus, 1995; Vieira et al., 1996; Seugnet et al., 1997; Strigini and Cohen, 2000). In the case of Dpp, endocytosis defective mutants (Bazinet et al., 1993; González-Gaitán and Jäckle, 1997) show a reduced Sal expression domain (González-Gaitán and Jäckle, 1999). GFP-Dpp punctate structures correspond to an endocytic compartment as indicated by colocalization of GFP-Dpp with internalized Texas-red dextran (Figures 4a–4c) (Masur et al., 1990). Therefore, we performed experiments to assess the endocytosis requirements in Dpp gradient formation. For this, we studied the effect on Dpp signaling of three established regulators of endocytic transport, such as Dynamin which regulates receptor internalization (Van der Bliek et al., 1993; Vieira et al., 1996) (Figures 4 and 5) and the two GTPases Rab5 and Rab7 (Figures 6 and 7) which regulate transport into early and late endosomes, respectively (Bucci et al., 1992; Méresse et al., 1995; Vitelli et al., 1997).

We blocked dynamin function using the thermosensitive mutant *shibire*^{ts1} (*shi*^{ts1}) (Chen et al., 1991) keeping the larvae at 34°C for 6 hr (Figures 4d–4g). In this experiment only the receiving cells lack dynamin function, whereas the secreting cells, rescued with a dpp-Gal4-driven functional *dynamin* transgene (Staples and Ramaswami, 1999), are able to perform endocytosis and express GFP-Dpp at normal levels (Figures 4d–4f). Texas-red dextran is not internalized by the Dpp receiving cells (Figure 4e) consistent with a block in endocytosis (Van der Bliek et al., 1993). When endocytosis is abolished, GFP-Dpp is only found as a weak, diffuse staining around the cells adjacent to the Dpp source (Figure 4g). No GFP-Dpp was internalized into endosomes (Figures 4d–4g), indicating that Dynamin-dependent endocytosis is essential for Dpp internalization.

To determine whether GFP-Dpp internalization involves receptor-mediated endocytosis, we monitored GFP-Dpp localization in *tkv*^{8} mutant clones which lack activity of the Dpp type I receptor Thickveins (Nellen et

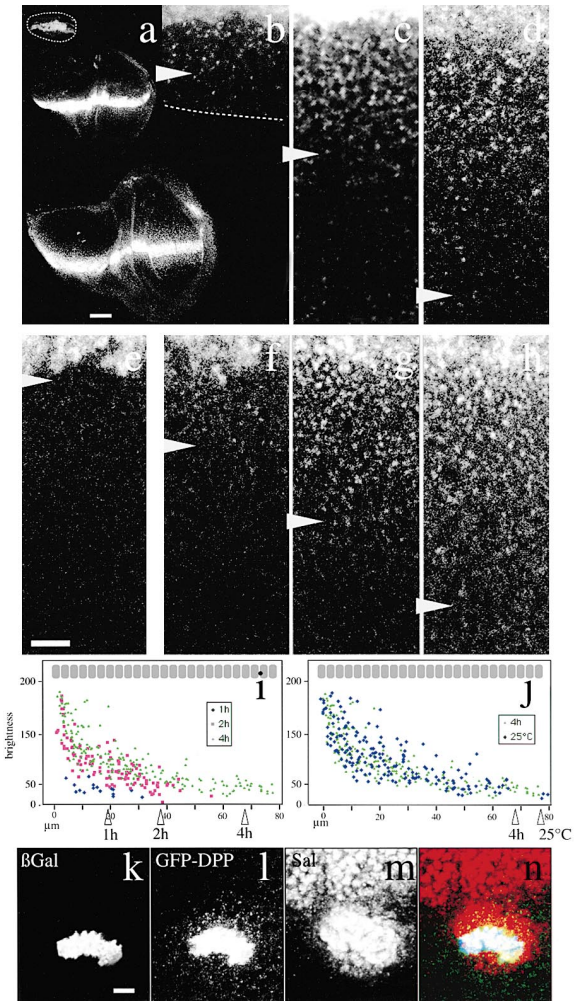

Figure 3. GFP-Dpp Dynamics

(a–d) GFP-Dpp distribution from the Dpp domain at second instar (60 hr after egg laying [AEL]; upper panel in a and b), early third instar (84 hr AEL; medium panel in a and c) and late third instar (120 hr AEL; lower panel in a and d). Dashed line: disc profile. (b–d) Magnification of the discs shown in (a). (e–h) GFP-Dpp propagation front. (e) GFP-Dpp distribution at 16°C. Note lack of GFP-Dpp in target tissue due to Gal4 thermosensitivity. A possible effect of temperature on gradient formation may take place as well. (f–h) GFP-Dpp distribution of different larvae kept at 16°C until third instar and shifted to 25°C during 1 (f), 2 (g), or 4 hr (h). Arrowheads, edge of the GFP-Dpp gradient (b–j). In (e)–(g) higher gain was applied to see dimmer GFP-Dpp. (i) Brightness versus distance to the source of punctate GFP-Dpp after 1 (blue), 2 (red) and 4 hr (green) at 25°C. (j) Brightness after 4 hr at 25°C (green) and in animals kept at 25°C (blue). (k–n) Triple labeling of a GFP-Dpp flip-out clone (see Experimental Procedures). (k) GFP-Dpp expressing cells labeled by cytosolic lacZ immunostaining. (l) GFP-Dpp. (m) Sal immunostaining. (n) Overlay. Note GFP-Dpp punctate structures and Sal around the expressing clone (l; yellow and green in n). Longer Sal activation range toward anterior is due to additive GFP-Dpp and Dpp signaling. Ten other clones showed the same behavior. Posterior: down. (b)–(h) are at the same magnification. Scale bars: 50 μm (a), 10 μm (b–h, k–n). The bar in (b)–(h) and (k)–(n) corresponds to around 3.3 cells.

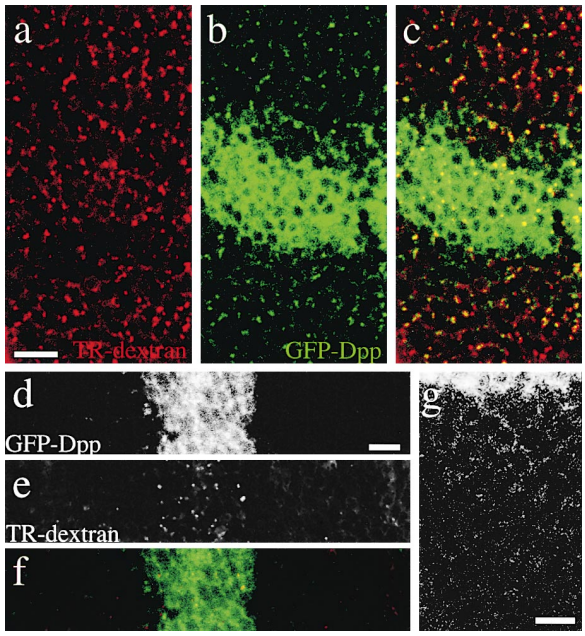

Figure 4. GFP-Dpp Endocytosis Is Dynamin-Dependent

(a–c) Double labeling showing internalized Texas-red dextran (a; 10 min pulse/20 min chase) and GFP-Dpp (b; *dpp-gal4/UAS-GFP-Dpp*). (c) Overlay. Note 95% colocalization in the receiving cells. (d–f) Double labeling showing GFP-Dpp (d) and internalized Texas-red dextran (e; 10 min pulse) from a *shi^{ts1}; UAS-Dynamin^{+}/+; dpp-gal4/UAS-GFP-Dpp* larva incubated at 34°C for 6 hr. (f) Overlay. Posterior: right. Note Texas-red dextran endocytosis only in the secreting cells (e). Before the block, GFP-Dpp was distributed in the normal gradient at the endosomes (not shown); after the block, is no longer present at endosomes in receiving cells. Heterozygous *shi^{ts1}*/+ siblings showed a normal GFP-Dpp distribution under these conditions (not shown). The mutant effects of the blockage are reversible. Note internalization of Texas-red dextran and GFP-Dpp in anterior cells (left side) adjacent to the Dpp domain due to perdurance of Dynamin^{+} driven by dpp-gal4 in previous cell generations. Note extracellular precipitated dye (posterior; right side) which is also occasionally observed upon incubation at 4°C. (g) GFP-Dpp distribution in a developing wing disc like the one shown in (d)–(f). Dpp expressing cells: up; posterior: down. Scale bars: 10 μm.

al., 1994). Cells were permeabilized to detect cytosolic β-galactosidase whose absence labels the *tkv^{8}* mutant cells. As a consequence most of the intracellular GFP-Dpp was washed off in these wing discs. In spite of this, GFP-Dpp is found around the mutant cells (Figures 5a–5d), suggesting that lack of Tkv causes an extracellular accumulation of Dpp. This implies that Dpp is internalized via Tkv receptor–mediated endocytosis.

Extracellular GFP-Dpp accumulated around the *tkv^{8}* cells facing the Dpp source, but was at much lower levels or absent in mutant cells behind them (Figures 5c and 5d). The extracellular accumulation of GFP-Dpp at the side facing the source suggests that it might be immobilized in the extracellular space and, thus, progresses only poorly further into the target tissue. Since the extracellular space cannot support long-range Dpp movement, gradient formation is likely to require Dpp internalization by dynamin-dependent endocytosis.

GFP-Dpp Propagation Requires Dynamin Activity

To test whether Dpp movement requires endocytosis, we generated *shi^{ts1}* mutant cell clones and asked whether Dpp progression is impaired. If Dpp progres-

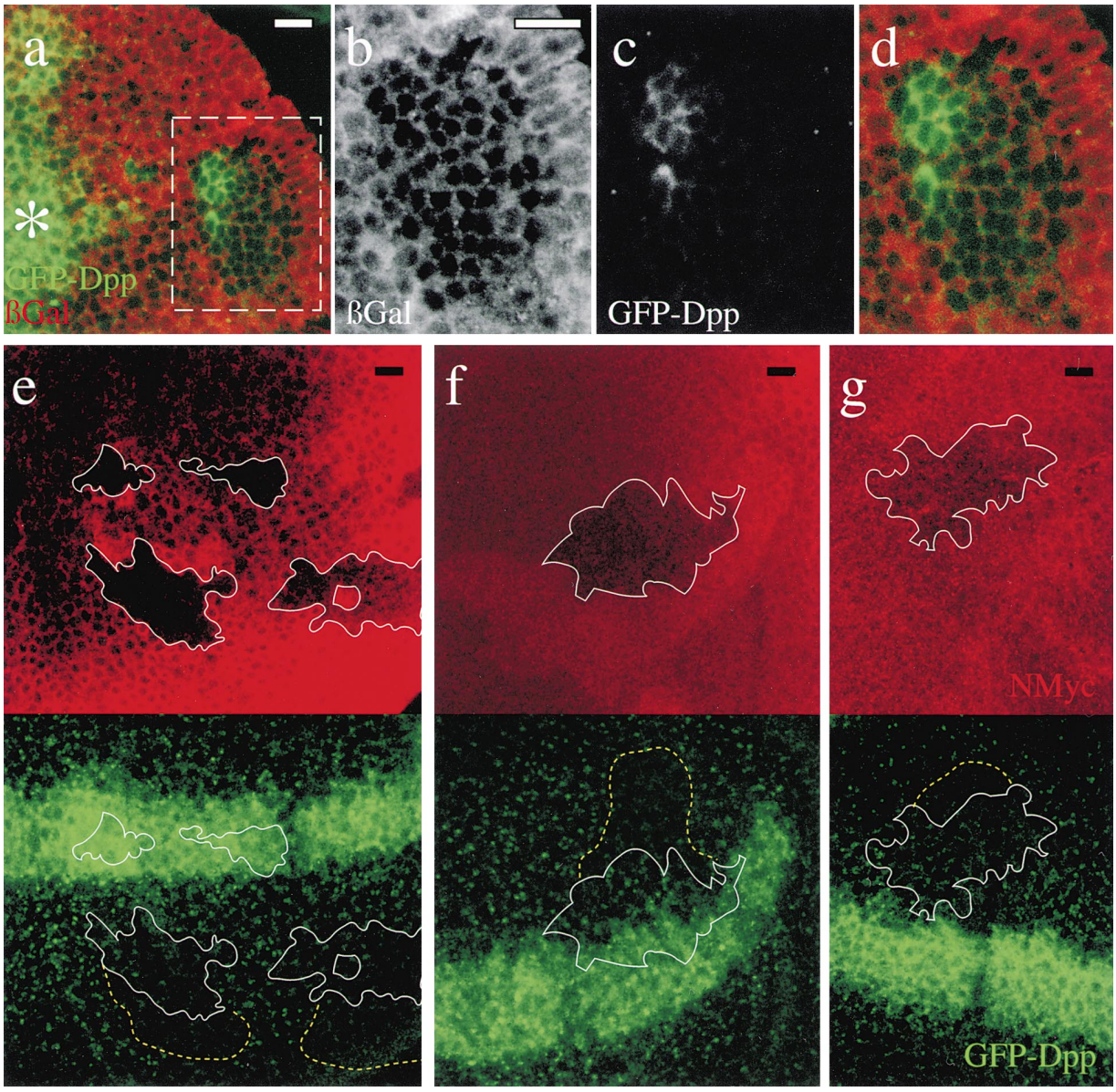

Figure 5. Thickveins and Dynamin Mutant Mosaics Impair Dpp Movement

(a) Double labeling showing GFP-Dpp (green) expressed from the Dpp domain (asterisk) and a *tkv*^{8} clone (66 cells) labeled by the absence of lacZ (red). (b)–(d) Magnification of the box in (a) showing the lacZ-lacking *tkv*^{8} clone (b), GFP-Dpp (c) and an overlay (d). Big *tkv*^{8} clones are only found far away from the source (Burke and Basler, 1996). Six clones showing the same behavior were observed. (e–g) Double labelings showing three examples of *shi*^{ts1} clones marked by the absence of NMyc (upper panels; red) and GFP-Dpp (lower panels; green). (e) Posterior clones. (f) Anterior clone also affecting the secreting cells. (g) Anterior clone. White line: clone outline; dotted yellow lines: approximate extent of the distal shadow with dimmer or no GFP-Dpp vesicular structures. A propagation front was started (14 hr, 29°C) followed by endocytosis block above *shi*^{ts1} restrictive temperature for 5 hr (see Experimental Procedures). Note few GFP-Dpp containing vesicles within the *shi*^{ts1} clones due to GFP-Dpp internalization at 29°C (a partially permissive temperature for *shi*^{ts1} developing wing cells; see Experimental Procedures). 15 clones with shadows were observed. In the Tkv and *shi*^{ts1} clones, receptor-mediated endocytosis was blocked during different periods of time (3 days versus 5 hr) explaining why extracellular accumulation of Dpp is not seen in the *shi*^{ts1} clone. Scale bars: 10 μm.

sion required Dynamin, cells behind the clone would not get Dpp from the mutant cells in the clone. However, since Dpp moves in all directions, the cells behind the clone can still receive Dpp through lateral and downstream neighbor cells (Figures 3e–3n). In this case, Dpp would be seen behind the *shi*^{ts1} clone, because Dpp will move rapidly from the surrounding cells and compensate for the lack of input from *shi*^{ts1} cells. As expected, hampered by the rapid and nondirectional movement of Dpp, we found GFP-Dpp behind the *shi*^{ts1} mutant clones (not shown). Consistent with the presence of both GFP-Dpp and endogenous Dpp behind these clones, expression of *sal* is also activated in cells behind the *shi*^{ts1} clones (not shown).

To uncover a possible effect of *shi*^{ts1} on Dpp progression through the mutant cells, we exploited the thermo-

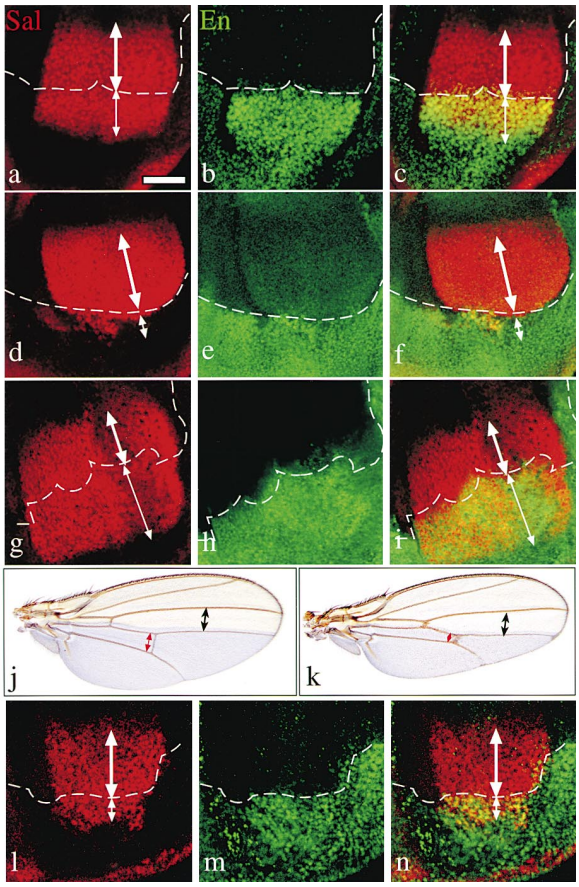

Figure 6. Dpp Signaling Range in Rab Mutants

(a–i) Double immunostaining showing Sal (a, d, and g) and Engrailed (b, e, and h) in wild-type (a–c), a disc expressing *DRab5S43N* in the posterior compartment (embryogenesis at 18°C; first instar, 8 hr at 29°C; larval development at 18°C) (d–f; *engrailed-gal4/UAS-DRab5S43N*) or overexpressing DRab5 at 29°C throughout development (g–i; *engrailed-gal4/UAS-DRab5*). (c, f, and i) Overlay. Dashed line: A/P boundary. Note Sal-activating Dpp signaling range in the anterior (thick arrow) and in the posterior compartment (thin arrow). Approximate range of Sal activation in posterior cells: wild-type, 15 cell diameters; *DRab5S43N*, 5 cells; DRab5 overexpression, up to 25 cells. (j) Wild-type wing. (k) Mutant wing from a disc expressing DRab7Q67L in the posterior cells (blue) at 16°C (*engrailed-gal4/UAS-DRab7Q67L*). Note compression of A/P axis of the P, but not the A compartment (cf. j versus k). Vein IV-V distance (red arrow): wild-type, 17.4 ± 2 cells; mutant: 5.9 ± 0.6 cells. Vein III-IV distance (control, black arrow): wild-type, 18.6 ± 1.3; mutant, 18.8 ± 1.3 cells. 8 wild-type and 8 mutant flies were quantified. (l–n) Double labeling showing Sal (l) and Engrailed immunostainings (m) in a mutant wing disc expressing DRab7Q67L in the posterior cells (blue) at 16°C (*engrailed-gal4/UAS-DRab7Q67L*). Range of Sal activation in the posterior cells is strongly reduced. Scale bar: 50 μm.

sensitivity of Gal4 and performed experiments where no GFP-Dpp is initially present in the target tissue (Figure 3e). We first generated *shi*^{ts1} cell clones which grew at a permissive temperature for *shi*^{ts1}, 16°C. We then pulsed GFP-Dpp expression from the source initiating a wave of Dpp propagation through the target tissue and subsequently blocked Dynamin at the restrictive temperature in the *shi*^{ts1} patch of cells (see Experimental Procedures). This way we challenged the progression of a Dpp wave with a Dynamin-defective region. If Dpp progression were Dynamin-dependent, cells behind the mutant clone would have to receive most GFP-Dpp from the upstream mutant cells when the leading edge of the GFP-Dpp wave passes through the clone. Figures 5e–5g show a lack of GFP-Dpp vesicles in the wild-type cells behind these *shi*^{ts1} clones ("shadows"). In this experiment, endogenous Dpp, unlike GFP-Dpp, must be present as a full-range gradient prior to blocking Dynamin. Therefore, endogenous Dpp will not form a shadow. This explains why *sal* is expressed in the area of the GFP-Dpp shadow (not shown), since cells behind the *shi*^{ts1} mutant clones received sufficient endogenous Dpp to maintain *sal* expression. This result indicates that lack of dynamin-dependent endocytosis impedes the progression of Dpp through the mutant clone.

We did not detect an effect on Dpp secretion in large *shi*^{ts1} cell clones located in the area of Dpp producing cells (not shown). This is in contrast to the proposed effect of *shi*^{ts1} on Wingless secretion (Strigini and Cohen, 2000). In any case, a possible effect of *shi*^{ts1} on Dpp secretion is irrelevant to explain the shadows observed in the area where cells do not produce Dpp, since we have shown that Dpp fails first to be internalized in cells lacking Dynamin.

The role of endocytosis during Dpp long-range movement suggests that Dpp trafficking through the endocytic pathway is essential for long-range gradient formation. Based on this, we predicted that Rab5 mutants would affect Dpp signaling range. The small GTPase Rab5 is required for formation of clathrin-coated vesicles (McLauchlan et al., 1998) and their subsequent fusion with early endosomes (Bucci et al., 1992; Stenmark et al., 1994). Like its mammalian counterpart, *Drosophila* Rab5 (DRab5) accumulates at the early endosome (not shown).

We expressed DRab5S43N, a dominant-negative mutant of Rab5 blocked at the inactive GDP-bound state (Stenmark et al., 1994), in posterior receiving cells using engrailed-Gal4. We could not visualize GFP-Dpp distribution when endocytic trafficking is impaired in receiving cells, because we cannot simultaneously drive *via* Gal4 GFP-Dpp in secreting cells and DRab5S43N in receiving cells. Instead, we monitored Dpp signaling range by Sal expression (Figures 6a–6i). Expression of DRab5S43N restricted the Sal expression to the cells adjacent to the Dpp source (Figures 6d–6f) indicating that impaired DRab5 function results in a reduced Dpp signaling range. Conversely, DRab5 overexpression in the receiving cells broadened the Sal expression domain, indicating an expansion of the Dpp signaling range (Figures 6g–6i). This indicates that endocytic trafficking is rate limiting for establishing of the Dpp signaling range, consistent with the role of endocytosis during Dpp gradient formation as shown above.

The Range of Dpp Signaling Is Controlled by Degradation

We have shown that the gradient is stable in spite of the rapid Dpp movement. We speculated that the gradient could be stable if a fraction of internalized Dpp is eliminated by degradation at the endocytic pathway in each receiving cell. In computer simulations where a wave of GFP-Dpp propagation is initiated (like in Figures 3e–3j),

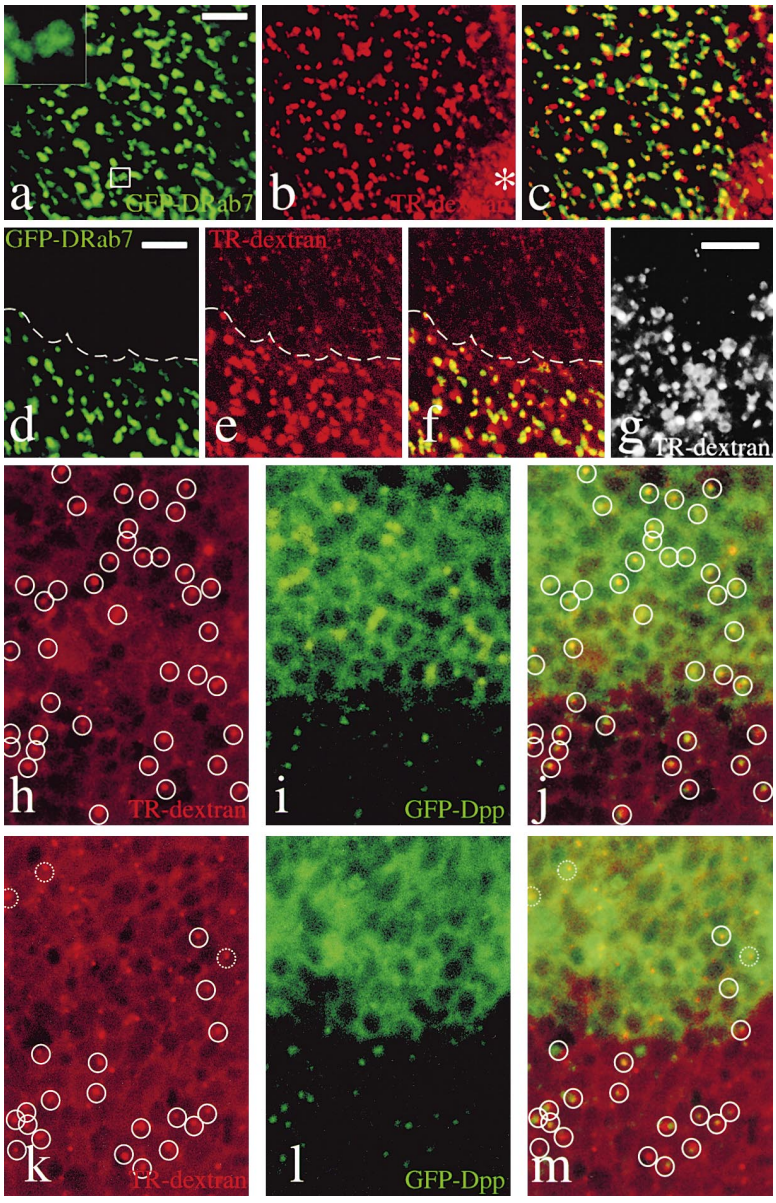

Figure 7. Sorting to the Late Endosome by DRab7

(a–c) Double labeling showing localization of GFP-DRab7 (a) at the late endosome (b) as visualized by Texas-red dextran internalization (5 min pulse/60 min chase; *engrailed-gal4/UAS-GFP-DRab7*). (c) Overlay. Note ring-shaped profile of the GFP-DRab7 membrane compartment (inset in a) and colocalization between GFP-DRab7 positive vesicular structures and late endosomes; colocalization is reduced to 10% between GFP-DRab7 and early endosomes (not shown). Asterisk in (b): apical unspecific trapping of Texas-red dextran (different focal plane). (d–f) Double labeling showing posterior overexpression of GFP-DRab7 (25°C; *engrailed-gal4/UAS-GFP-DRab7*) (d) and late endosomes (e). Dashed lines: A/P compartment boundary. (f) Overlay. Posterior: down. Note late endosomal accumulation of Texas-red dextran in DRab7 overexpressing cells, when compared to anterior cells. Accumulation of Texas-red dextran in early endocytic compartments (5 min pulse) is reduced in cells overexpressing DRab7 (not shown). (g) Enlarged late endosomes detected by the Texas-red dextran pulse/chase protocol in DRab7Q67L posterior expressing cells at 25°C (*engrailed-gal4/UAS-DRab7Q67L*). Posterior: down. Scale bars: 10 μm. (h–j) Double staining showing internalized Texas-red dextran (h; 10 min pulse/20 min chase) and GFP-Dpp (i) at the secreting (up) and the receiving cells (down). (j) overlay. Genotype *dpp-gal4/UAS-GFP-Dpp*. Circles: colocalization of brighter GFP-Dpp-positive vesicular structures and the endosome labeled by internalized Texas-red dextran. (k–m) Double staining showing internalized Texas-red dextran (k, same protocol) and GFP-Dpp (l) in a disc where DRab7Q67L was pulsed (from 18°C; 25°C, 30 hr; *UAS-DRab7Q67L/+; dpp-gal4/UAS-GFP-Dpp*) in the secreting cells. (m) overlay. Note only a few spots of internalized GFP-Dpp at the DRab7Q67L expressing cells. Circles: Texas-red dextran positive structures containing GFP-Dpp. Dotted circles: positions where instead of precise colocalization, internalized Texas-red dextran dots are within a blob of GFP-Dpp. Note that no enlarged endosomes at the secreting cells were seen due to lower levels of DRab7Q67L in this experiment than in the one shown in (g).

a low percentage of degradation in each cell (5%) allowed for a rapid expansion of the gradient, which shortly after initiation of the wave expands asymptotically and reaches a steady state (not shown). In the simulations, no differential degradation rate in space or time needs to be imposed to generate a stable gradient. In this scenario the rate of degradation determines how much Dpp is passed to the next cells defining thereby the steady-state slope of the gradient and the range of signaling.

To test this prediction, we generated a mutant of the small GTPase Rab7 (DRab7). It is well established that Rab7 targets endocytic cargo from the early to the late endosome and lysosome for degradation (Méresse et al., 1995; Vitelli et al., 1997). DRab7 accumulates at a ring-shaped late endosomal structure in the developing wing cells, as revealed by colocalization of GFP-DRab7 and Texas-red dextran internalized into a late endosomal compartment (Figures 7a–7c). Furthermore, overexpression of GFP-DRab7 causes enhanced late endosomal sorting of Texas-red dextran (Figures 7d–7f). This phenotype is enhanced by the expression of DRab7Q67L (Figure 7g), a dominant gain-of-function mutant blocked in the active GTP-bound state (Méresse et al., 1995; Vitelli et al., 1997). This indicates that DRab7 controls the sorting of endocytic cargo toward the late endosome. DRab7 mutants can therefore serve as a tool to study late endosomal trafficking of Dpp and to establish the role of this trafficking step in Dpp signaling.

We addressed whether expression of DRab7Q67L

causes enhanced degradation of Dpp. In wild-type secreting cells, endocytosed GFP-Dpp accumulates in vesicular structures which colocalize with internalized Texas-red dextran (Figures 7h–7j). GFP-Dpp can also be detected both in the cytoplasm and in vesicular structures which do not colocalize with Texas-red dextran (Figures 7i and 7j) corresponding to GFP-Dpp which is trafficking through the secretory pathway. We coexpressed GFP-Dpp and DRab7Q67L in the secreting cells. In these cells, cytosolic GFP-Dpp is found at normal levels, whereas internalized GFP-Dpp is found at much lower levels and cannot be distinguished from cytosolic GFP-Dpp (Figures 7k–7m). Furthermore, endocytosed GFP-Dpp is found in the receiving cells which do not express DRab7Q67L, indicating that secretion of GFP-Dpp from the DRab7Q67L cells is not affected (Figures 7k–7m). This is consistent with the proposal that degradation of endocytosed GFP-Dpp is dependent on DRab7 activity.

In posterior receiving cells, ectopic expression of DRab7Q67L caused an anterior/posterior compression of the venation pattern and shape of the posterior compartment (Figures 6j and 6k), suggesting a reduction of the functional range of Dpp signaling. As with DRab5, we could not monitor directly the distribution of Gal4-driven GFP-Dpp under these conditions of enhanced degradation in the receiving cells. We therefore monitored Dpp signaling range by looking at Sal (Figures 6l–6n). Expression of DRab7Q67L in receiving cells causes a reduction of the Sal expression domain (Figures 6l–6n), indicating that sorting of endocytic cargo toward degradation limits the range of Dpp signaling. This suggests that Dpp degradation restricts the signaling range, a hypothesis we will test as soon as Gal4 independent GFP-Dpp expression is available.

Discussion

During pattern formation and organogenesis, positional information is encoded by the graded distribution of morphogen activity. Are morphogens distributed in concentration gradients? How do they move through the tissue? What cellular and molecular factors control morphogen movement so that they can form gradients? To address these key questions we have monitored the distribution of a functional GFP-Dpp. We found that Dpp is indeed distributed as a long-range concentration gradient which explains the long-distance activation of the target genes *sal* and *omb*. This supports a long-standing model in which long-range morphogens encode positional information by forming concentration gradients (Wolpert, 1969). Dpp moves without preferential direction at a speed of more than 4 cells per hour through the target tissue. Interestingly, in spite of the rapid movement of Dpp, the shape of the gradient remains stable. We have shown that Dpp extracellular diffusion alone does not explain its distribution as a stable gradient and that receptor-mediated endocytosis is essential for Dpp long-range movement. This is based on three observations. (1) sGFP fails to form a stable gradient by simple diffusion; (2) Dpp is internalized by Dynamin-dependent endocytosis and fails to move across a Dynamin-defective clone of cells, forming a shadow behind it; and (3) when Dpp progression is confronted with a clone of cells lacking Tkv, extracellular Dpp accumulates as it enters the clone and does not progress further into it. The effect of DRab5 and DRab7 mutants on the range of activation of the Dpp target gene Spalt indicates that endocytic trafficking plays an essential, rate limiting role for establishing the Dpp signaling range.

Models of Dpp Transmission

Several models have been invoked to explain the distribution of morphogens to form concentration gradients. Cell proliferation, free diffusion, restricted diffusion and planar transcytosis have all been considered to play key roles in different models of gradient formation (Bejsovec and Wieschaus, 1995; McDowell et al., 1997; Pfeiffer et al., 2000; reviewed in Strigini and Cohen, 1999).

In the case of Wingless (Wg), it has been reported that this ligand can be retained at the secretory pathway several cell generations after its transcription (Pfeiffer et al., 2000). Based on this, it has been suggested that the Wg gradient is formed upon cell proliferation as the progeny of the expressing cells is pushed away from the source thereby stopping Wg activation. Cell proliferation cannot account for Dpp gradient formation, since it takes longer for a developing wing cell to divide once (8 hr) (Garcia-Bellido, 1972; Gonzalez-Gaitan et al., 1994) than for the tissue to form a full-range gradient (Figures 3e–3j).

In the case of Activin, diffusion has been proposed as the main mechanism explaining the formation of a 300 μm wide gradient in tissue culture (Gurdon et al., 1994). In the developing wing, diffusion of the sGFP through the extracellular space fills a target field of 120 μm and cannot generate a stable gradient. In contrast, the distribution of Dpp is specifically restricted. Thus, 8 hr after the GFP-Dpp pulse, the gradient reaches its full range and does not expand further, indicating that Dpp movement is limited. Consistently, in the cell clones lacking Tkv activity, Dpp accumulates at the side facing the source and does not progress further, also suggesting restricted Dpp movement at the extracellular space. Furthermore, in contrast to sGFP which fills the extracellular space, extracellular Dpp is only observed adjacent to the source. It is still possible that lower levels of extracellular Dpp farther away from the source are present, but undetectable. In any case, these observations indicate that extracellular factors act specifically on secreted Dpp and prevent its unlimited diffusion.

Diffusion might be restricted by trapping of Dpp when bound to extracellular matrix components such as the proteoglycan Dally (Jackson et al., 1997). This may account for the suppressor effect of *dpp* mutations on *dally* mutants in the wing, a possibility we are currently investigating by using GFP-Dpp. In addition, the Dpp receptor Tkv may also contribute to titrate the ligand (Lecuit and Cohen, 1998). However, factors other than Tkv must also be involved in the restricted diffusion of Dpp, since extracellular Dpp movement is limited in the Tkv mutant clones. Another mechanism to limit Dpp diffusion would be its internalization by endocytosis. This does not seem to be a major factor, since the endocytosis-defective shi^{ts1} cell clones impair rather than facilitate Dpp progression. Furthermore, in the

DRab5 dominant-negative mutants, Dpp signaling range is reduced. Still another alternative would be that a factor degrades Dpp in the extracellular space, thereby limiting its long-range diffusion. This factor however would not impede Dpp extracellular accumulation in the Tkv mutant clones.

Another model of gradient formation, also proposed for Wg (Bejsovec and Wieschaus, 1995), involves intracellular trafficking by planar transcytosis through the receiving cells. In the model, Wg is internalized by endocytosis, traffics intracellularly and is released to signal in the next cells, which in turn internalize it and release it as well. This way the ligand moves further through the target tissue. Our data showing the accumulation of GFP-Dpp at the side facing the source in the cell clones lacking Tkv and the lack of GFP-Dpp behind the Dynamin-defective clones suggest that receptor-mediated endocytosis of Dpp is essential for the long-range gradient formation. We observed nondirectional rapid movement of Dpp in the wing epithelium. Therefore, we do not predict any stable shadow behind the *shi^{ts1}* clones. Consistent with this, we can see shadows only under dynamic conditions, when confronting a wave of GFP-Dpp with the *shi^{ts1}* mutant clone. Thus, visualization of GFP-Dpp while traveling through the tissue revealed a role for endocytosis during Dpp transmission which would not have been possible by looking only at expression of the target genes. Our data are therefore consistent with a model where Dpp diffusion is limited by extracellular factors and its long-range distribution is mediated by planar transcytosis initiated by Dpp endocytosis.

Control of Dpp Signaling at the Endocytic Pathway

The Rab mutant analysis reveals that the range of Dpp signaling is controlled by endocytic trafficking and degradation in the receiving cells. This finding is consistent with three possible scenarios which do not exclude each other. (1) The Dpp receptor is downregulated by degradation in the DRab7 gain-of-function mutant, whereas its recycling is impaired or enhanced in the DRab5 dominant-negative and overexpression conditions, respectively. In this case, the Dpp signaling range can be changed without affecting the actual distribution of the ligand. (2) Dpp internalization by endocytosis carries the ligand to an endosomal compartment where the actual signal transduction takes place. This possibility is consistent with recent reports showing that during TGF-β signal transduction, the FYVE-domain protein SARA recruits the transcription factor Smad2 to an intracellular compartment and presents it there to the internalized TGF-β receptor complex (Tsukazaki et al., 1998). (3) Dpp travels intracellularly through the endocytic pathway through planar transcytosis. Our data suggest a DRab7-dependent degradation of Dpp. In the DRab7 gain-of-function mutant, enhanced degradation might reduce the range of Dpp progression by planar transcytosis. In the DRab5 dominant-negative mutant, the endocytic trafficking of Dpp would be impaired, whereas it would become more effective in DRab5 overexpression situation, increasing the rate of endocytic trafficking and therefore Dpp transcytosis and range of distribution.

We favor a model where the balance between recycling and degradation of the ligand in the endocytic pathway determines the shape of the gradient. In this model, establishment and maintenance of the gradient do not require a differential rate of endocytosis and/or degradation of the ligand. The same rate of degradation in all receiving cells is sufficient to account for gradient formation. Similarly, the slow expansion of the gradient during development might reflect a slow increase in the number of Dpp producing cells rather than a change in the kinetics of trafficking.

The model implies that the target cells do not only interpret the gradient, but also contribute to determine its slope and shape. This would allow modulation of both the shape and size of different organs during development and evolution. Thus, a change in the ratio between recycling and degradation of the ligand either locally or globally in a given target tissue will yield changes in organ shape and size, respectively. This ratio could in turn be adjusted by the relative activity of Rab proteins controlling the recycling (Rab4, Rab5, and Rab11) and degradation (Rab7) of the endocytic cargo (reviewed in Olkkonen and Stenmark, 1997), a possibility which we will explore in the future.

Experimental Procedures

Mutant Strains

In(2L)dpp^{d12}, *Df(2L)dpp^{d14}*, *shi^{ts1}*, *tkv^{8}* and other mutants used are described in Flybase. *tkv^{8}* is a Tkv receptor truncated at amino acid 144 before the transmembrane domain (Nellen et al., 1994). In UAS-GFP-Dpp, EGFP was cloned into the codon 465 in the Dpp cDNA. In Western blot experiments with *dpp-gal4/UAS-GFP-Dpp* wing discs using anti-GFP antibodies (Brock et al., 1999), a single 42 kDa band was observed as predicted for secreted GFP-Dpp. UAS-sGFP (37 kDa) was generated from GFP-Dpp by deletion of 4 base pairs at the GFP C terminus causing a frameshift. *UAS-Dynamin* flies carry a cDNA (GS23121; BDGP) coding for the DynaminΔ2S splicing variant (Staples and Ramaswami, 1999). DRab7 (cDNA GH03685, BDGP; AF263363, gi:3426325) shares 84% similarity with Human Rab7 and 94% similarity in the case of the N-terminal constant region (amino acids 1–163). GFP-DRab7, is an N-terminal GFP fusion. UAS-DRab5 contains a DRab5 cDNA (GM02432; BDGP). UAS-DRab7Q67L and UAS-DRab5S43N were generated by in vitro mutagenesis.

GFP-Dpp Rescue

dpp^{d12}/CyO, Act-GFP; dpp-gal4/+ were crossed to *dpp^{d14}/CyO, Act-GFP; UAS-GFP-Dpp/+*. The *dpp^{d12}/dpp^{d14}; dpp-gal4/UAS-GFP-Dpp* larvae were identified by Gal4-driven GFP-Dpp present at the salivary glands and lack of ubiquitous GFP. For rescue to adulthood, animals were raised at 16°C to minimize ectopic gal4-dependent overexpression.

Immunostaining and Imaging of GFP-Dpp

Immunostainings were performed as previously described (González-Gaitán and Jäckle, 1996) using Mouse anti-Engrailed (4D9; Hybridoma Bank), 1:500 dilution; Rabbit anti-Spalt (Kühnlein et al., 1994), 1:25; Mouse anti-β-Gal, 1:50; Mouse anti-Myc, 1:75; Mouse anti-GFP, 1:12. GFP-Dpp was imaged either in vivo (M3 medium) or after fixation (4% PFA); no difference was observed. Fewer and dimmer punctate structures were found upon immunostaining due to detergents which washed out GFP-Dpp from the endosomal lumen. Extracellular GFP-Dpp was detected by incubation with anti-GFP antibody prior to fixation (Strigini and Cohen, 2000). To estimate GFP-Dpp range in number of cell diameters either an extracellular Texas-red dextran counterstaining was performed to monitor the cell profiles or distance was measured and converted into cell numbers (2.96 ± 0.28 μm/cell; 5 μm below apical pole). Average cell size was estimated by counting cells across 20 μm long segments (50 segments; 5 discs). To see the cell profiles, extracellular dextran

was monitored by applying 1 min 0.5 mM Texas-red dextran, immediately washing and fixing.

Mosaics

GFP-Dpp flip-out clones (Pignoni and Zipursky, 1997) were generated by heat shock (90 min, 37°C) in second instar larvae (*HS-Flp/Act>CD2>Gal4; UAS-lacZ/UAS-GFP-Dpp*). *tkv*^{8} mutant Minute^{+}/FRT clones (Xu and Harrison, 1994) were generated by heat shock (90 min, 37°C) in 4 days old larvae (*HS-Flp/+; M(2)z arm-lacZ FRT40A/tkv*^{8} *FRT40A; dpp-gal4/UAS-GFP-Dpp*) and their mid-third instar discs were fixed. *shi*^{ts1} FRT mutant clones were generated in larvae of the genotype *shi*^{ts1} *FRT18A/HS-NM8A FRT18A; HS-Flp/+; dpp-gal4/UAS-GFP-Dpp*. After one day embryo collection (18°C), larvae were raised at 25°C for one day and heat shocked (90 min, 38°C plus 120 min, 22°C). Larvae were subsequently kept at 16°C until third instar larval stage. Afterwards, a propagation front was initiated by incubating the larvae at 29°C for 14 hr. Under these conditions the full-range gradient is formed after more than 8 hr due to partial dominance of *shi*^{ts1} (Grant et al., 1998). Then, we blocked endocytosis for 2 hr at 34°C followed by 1 hr at 38°C to induce both NMyc transcription and shibire block and 2 hr at 34°C to allow the translation of the NMyc transcript. Dissection of the discs was at 34°C and fixation on ice. 5 to 10 apical confocal sections were projected to compile vesicular structures in different Z levels.

Endocytosis Assays

Third instar larval discs were incubated in 0.5 mM Texas-red dextran (lysine fixable, MW3000; Molecular Probes) in M3 medium at 25°C (pulse) and then washed 5 times for 2 min with ice-cold M3 medium. The apical epithelial side is immediately accessible to Texas-red dextran. Afterwards they were either fixed in paraformaldehyde (20 min, room temperature) or incubated at 25°C for various periods of time (chase) and fixed. To visualize the endocytic compartments, discs were pulsed for 10 min and chased for 20 min; for late endosomes, 5 min pulse and 60 min chase. To monitor endocytosis, 10 min pulse and immediate fixation. At 16°C, 25°C, and 29°C, wild-type and *shi*^{ts1} wing cells internalize Texas-red dextran upon a 10 min pulse. Complete block of endocytosis in *shi*^{ts1} occurs above 34°C, while wild-type wing cells can internalize at this temperature.

Blockage of Endocytosis at Receiving Cells

shi^{ts1}*; UAS-Dynamin*$^{+}$*/+; dpp-gal4/UAS-GFP-Dpp* larvae were kept at the *shi*^{ts1} permissive temperature (25°C or 16°C) to allow normal wing development until third instar larva when endocytosis was blocked for 6 hr at 34°C. Wing discs were dissected and incubated for 10 min with Texas-red dextran at 34°C, washed on ice, and fixed.

Acknowledgments

We thank H. Taubert and R. Fernández de la Fuente for excellent technical assistance; G. Dowe, R. Rivera, D. Kötting, T. Wucherpfennig, K. Müller, and E. González for their various contributions; K. Basler and R. Schuh for sharing reagents; H. Jäckle, M. Zerial, S. Eaton, F. Schweisguth, J. Smith, L. Wolpert, W. Huttner, A. Ferrús, B. Linder, W. Gerber, and O. Piepenburg for comments to the manuscript; N. Dimopoulos for initial work on DRab7. The work was supported by the Max-Planck Society and a DFG grant to M. G.-G.

Received October 12, 2000; revised November 11, 2000.

References

Basler, K., and Struhl, G. (1994). Compartment boundaries and the control of *Drosophila* limb pattern by Hedgehog protein. Nature *368*, 208–214.

Bazinet, C., Katzen, A.L., Morgan, M., Mahowald, A.P., and Lemmon, S.K. (1993). The *Drosophila clathrin heavy chain* gene function is essential in a multicellular organism. Genetics *134*, 1119–1134.

Bejsovec, A., and Wieschaus, E. (1995). Signaling activities of the *Drosophila wingless* gene are separately mutable and appear to be transduced at the cell surface. Genetics *139*, 309–320.

Brand, A., Manoukian, A.S., and Perrimon, N. (1996). Ectopic expression in *Drosophila*. In *Drosophila melanogaster*: Practical Uses in Cell and Molecular Biology, L.S.B. Goldstein and E.A. Fyrberg, eds. (San Diego, CA: Academic Press), pp. 635–654.

Brock, R., Hamelers, I.H.L., and Jovin, T.M. (1999). Comparison of fixation protocols for adherent cultured cells applied to a GFP fusion protein of the Epidermal Growth Factor Receptor. Cytometry *35*, 353–362.

Bryant, P.J. (1988). Localized cell death caused by mutations in a *Drosophila* gene coding for a transforming growth factor-β homolog. Dev. Biol. *128*, 386–395.

Bucci, C., Parton, R.G., Mather, I.H., Stunnenberg, H., Simons, K., Hoflack, B., and Zerial, M. (1992). The small GTPase rab5 functions as a regulator factor in the early endocytic pathway. Cell *70*, 715–728.

Burke, R., and Basler, K. (1996). Dpp receptors are autonomously required for cell proliferation in the entire developing wing. Development *122*, 2261–2269.

Chen, M.S., Obar, R.A., Schroeder, C.C., Austin, T.W., Poodry, C.A., Wadsworth, S.C., and Vallee, R.B. (1991). Multiple forms of Dynamin are encoded by *shibire*, a *Drosophila* gene involved in endocytosis. Nature *351*, 583–586.

Cui, Y., Jean, F., Thomas, G., and Christian, J.L. (1998). BMP-4 is proteolytically activated by furin and/or PC6 during vertebrate embryonic development. EMBO J. *17*, 4735–4743.

Garcia-Bellido, A. (1972). Some parameters of mitotic recombination in *Drosophila melanogaster*. Mol. Gen. Genet. *115*, 54–72.

González-Gaitán, M.A.F., Capdevila, M.P., and Garcia-Bellido, A. (1994). Cell proliferation patterns in the wing imaginal disc of *Drosophila*. Mech. Dev. *46*, 183–200.

González-Gaitán, M.A., and Jäckle, H. (1996). *In situ* localization of proteins in whole mounted tissue. In The Molecular Biology of Insect Disease Vectors: A Methods Manual, J.M. Crampton, C.B. Beard, and C. Lewis, eds. (London: Chapmann and Hall), pp. 283–294.

González-Gaitán, M.A., and Jäckle, H. (1997). Role of *Drosophila* α-adaptin during synaptic vesicle recycling. Cell *88*, 767–776.

González-Gaitán, M.A., and Jäckle, H. (1999). The range of *spalt*-activating Dpp signalling is reduced in endocytosis-defective *Drosophila* wing discs. Mech. Dev. *87*, 143–151.

Grant, D., Unadkat, S., Katzen, A., Krishnan, K.S., and Ramaswami, N. (1998). Probable mechanisms underlying interallelic complementation and temperature sensitivity of mutations at the *shibire* locus of *Drosophila melanogaster*. Genetics *149*, 1019–1030.

Green, J.B., and Smith, J.C. (1990). Gradient changes in dose of a *Xenopus* Activin A homologue elicit stepwise transition in embryonic cell fate. Nature *347*, 391–394.

Gurdon, J.B., Harger, P., Mitchell, A., and Lemaire, P. (1994). Activin signalling and response to a morphogen gradient. Nature *371*, 487–492.

Ingham, P.W., and Fietz, M.J. (1995). Quantitative effects of Hedgehog and Decapentaplegic activity on the patterning of the *Drosophila* wing. Curr. Biol. *5*, 432–440.

Jackson, S.M., Nakato, H., Sugiura, M., Jannuzi, A., Oakes, R., Kaluza, V., Golden, C., and Selleck, S.B. (1997). dally, a *Drosophila* glypican, controls cellular responses to the TGF-β-related morphogen Dpp. Development *124*, 4113–4120.

Kühnlein, R.P., Frommer, G., Friedrich, M., González-Gaitán, M.A.F., Wagner-Bernholz, J.F., Gehring, W.J., Jaeckle, H., and Schuh, R. (1994). *spalt* encodes an evolutionarily conserved zinc finger protein of novel structure which provides homeotic gene function in the head and tail region of the *Drosophila* embryo. EMBO J. *13*, 168–179.

Lecuit, T., and Cohen, S.M. (1998). Dpp receptor levels contribute to shaping the Dpp morphogen gradient in the *Drosophila* wing imaginal disc. Development *125*, 4901–4907.

Lecuit, T., Brook, W.J., Ng, M., Calleja, M., Sun, H., and Cohen, S.M. (1996). Two distinct mechanisms for long-range patterning by decapentaplegic in the *Drosophila* wing. Nature *381*, 387–393.

Masucci, J.D., Miltenberger, R.J., and Hoffmann, F.M. (1990). Pattern-specific expression of the *Drosophila decapentaplegic* gene is regulated by cis-regulatory elements. Genes Dev. *4*, 2011–2023.

Masur, S.K., Kim, Y.T., and Wu, C.F. (1990). Reversible inhibition

of endocytosis in cultured neurons from *Drosophila* temperature-sensitive mutant *shibire^{ts1}*. J. Neurogenet. *6*, 191–206.

McDowell, N., Zorn, A.M., Crease, D.J., and Gurdon, J.B. (1997). Activin has direct long-range signalling activity and can form a concentration gradient by diffusion. Curr. Biol. *7*, 671–681.

McLauchlan, H., Newell, J., Morrice, N., Osborne, A., West, M., and Smythe, E. (1998). A novel role for Rab5-GDI in ligand sequestration into clathrin-coated pits. Curr. Biol. *8*, 34–45.

Méresse, S., Gorvel, J.P., and Chavrier, P. (1995). The Rab7 GTPase resides on a vesicular compartment connected to lysosomes. J. Cell. Sci. *108*, 3349–3358.

Nellen, D., Affolter, M., and Basler, K. (1994). Receptor serine/threonine kinases implicated in the control of the *Drosophila* body pattern by decapentaplegic. Cell *78*, 225–237.

Nellen, N., Burke, R., Struhl, G., and Basler, K. (1996). Direct and long-range action of a DPP morphogen gradient. Cell *85*, 357–368.

Olkkonen, V.M., and Stenmark, H. (1997). Role of Rab GTPases in membrane traffic. Int. Rev. Cytol. *176*, 1–85.

Padgett, R.W., St. Johnston, R.D., and Gelbart, W.M. (1987). A transcript from a *Drosophila* pattern gene predicts a protein homologous to the transforming growth factor β family. Nature *325*, 81–84.

Panganiban, G.E.F., Rashka, K.E., Neitzel, M.D., and Hoffmann, F.M. (1990). Biochemical characterization of the *Drosophila* Dpp protein a member of the transforming growth factor beta family of growth factors. Mol. Cell. Biol. *10*, 2669–2677.

Pfeiffer, S., Alexandre, C., Calleja, M., and Vincent, J.P. (2000). The progeny of *wingless*-expressing cells deliver the signal at a distance in *Drosophila* embryos. Curr. Biol. *10*, 321–324.

Pignoni, F., and Zipursky, S.L. (1997). Induction of *Drosophila* eye development by decapentaplegic. Development *124*, 271–278.

Ramírez-Weber, F.A., and Kornberg, T.B. (1999). Cytonemes: cellular processes that project to the principal signaling center in *Drosophila* imaginal Discs. Cell *97*, 599–607.

Seugnet, L., Simpson, P., and Haenlin, M. (1997). Requirement for *dynamin* during Notch signaling in *Drosophila* neurogenesis. Dev. Biol. *192*, 585–598.

Staples, R.R., and Ramaswami, M. (1999). Functional analysis of Dynamin in *Drosophila melanogaster*. J. Neurogenet. *13*, 119–143.

Stenmark, H., Parton, R.G., Steele-Mortimer, O., Luetcke, A., Gruenberg, J., and Zerial, M. (1994). Inhibition of rab5 GTPase activity stimulates membrane fusion in endocytosis. EMBO J. *13*, 1287–1296.

Strigini, M., and Cohen, S.M. (1999). Formation of morphogen gradients in the *Drosophila* wing. Semin. Cell. Dev. Biol. *10*, 335–344.

Strigini, M., and Cohen, S.M. (2000). Wingless gradient formation in the *Drosophila* wing. Curr. Biol. *10*, 293–300.

Tsukazaki, T., Chiang, T.A., Davidson, A.F., Attisano, L., and Wrana, J.L. (1998). SARA, a FYVE domain protein that recruits Smad2 to the TGFbeta receptor. Cell *95*, 779–791.

Turing, A.M. (1952). The chemical basis of morphogenesis. Philos. Trans. R. Soc. (Lond.) *237*, 37–72.

Van der Bliek, A.M., Redelmeier, T.E., Damke, H., Tisdale, E., Meyerowitz, E.M., and Schmid, S. (1993). Mutations in human dynamin block an intermediate stage in coated vesicle function. J. Cell Biol. *122*, 553–563.

Vieira, A.V., Lamaze, C., and Schmid, S.L. (1996). Control of EGF receptor signaling by Clathrin-mediated endocytosis. Science *274*, 2086–2089.

Vitelli, R., Santillo, M., Lattero, D., Chiariello, M., Bifulco, M., Bruni, C.B., and Bucci, C. (1997). Role of the small GTPase Rab7 in the late endocytic pathway. J. Biol. Chem. *272*, 4391–4397.

Wolpert, L. (1969). Positional information and the spatial pattern of cellular differentiation. J. Theor. Biol. *25*, 1–47.

Xu, T., and Harrison, S.D. (1994). Mosaic analysis using FLP recombinase. In Drosophila melanogaster: Practical Uses in Cell and Molecular Biology, L.S.B. Goldstein and E.A. Fyrberg, eds. (San Diego, CA: Academic Press), pp. 655–681.